emerald PUBLISHING

Rapid Prototyping J

# Process Parameter Influence on Geometric Accuracy of Nylon 12 Parts Manufactured by FFF



| | |
|---|---|
| Journal: | *Rapid Prototyping Journal* |
| Manuscript ID | RPJ-03-2025-0101.R2 |
| Manuscript Type: | Original Article |
| Keywords: | Additive manufacturing, Fused filament fabrication, Geometrical deviations, Geometrical errors, Nylon, Surface roughness |
| | |

# Process Parameter Influence on Geometric Accuracy of Nylon 12 Parts Manufactured by FFF

**Keywords:** Additive manufacturing, Fused filament fabrication, Geometrical deviations, Geometrical errors, Nylon, Roughness

**Paper type** Research paper

**Abstract**

**Purpose**: This study analyzes the influence of extrusion temperature, printing speed, and layer thickness on dimensional accuracy, geometric deviations, and surface roughness of Nylon 12 parts fabricated via Fused Filament Fabrication (FFF). Understanding these effects is key to optimizing the process for precision engineering and biofabrication applications.

**Design/methodology/approach**: Hollow cylindrical specimens were printed under varying conditions: extrusion temperature (240–270 °C), printing speed (40–60 mm/s), and layer thickness (0.1–0.3 mm). Dimensional deviations, roundness, circular run-out, cylindricity, straightness, and surface roughness were analyzed. Response Surface Methodology (RSM) was applied to develop predictive models, while Grey Relational Analysis (GRA) was used to optimize process parameters.

**Findings**: Higher layer thickness and extrusion temperature increased surface roughness, while higher printing speeds worsened roundness and cylindricity but improved straightness and circular run-out. The optimal parameters identified by GRA were 40 mm/s speed, 0.1 mm layer thickness, and 255 °C extrusion temperature.

**Originality/value**: This study systematically evaluates geometric deviations in Nylon 12 parts fabricated via FFF, an area with limited prior research. The combined use of RSM and GRA provides a robust approach to minimize geometric errors and enhance print quality, benefiting industries requiring high-precision polymer components, such as aerospace, biomedical engineering, and mechanical manufacturing.

## Acronyms

FFF = Fused Filament Fabrication

$v$ = Printing speed (mm/s)

$T$ = Extrusion temperature (°C)

$e$ = Layer thickness (mm)

$D_{ou}$ = Outer diameter deviation

$D_{in}$ = Inner diameter deviation

$H$ = Height deviation

*RON* = Roundness deviation

*CRO* = Circular runout

*STR* = Straightness deviation

*CYL* = Cylindricity deviation

*Ra* = Arithmetic mean surface roughness (µm)

$l_s$ = Scan length (µm)

$l_c$ = Contact length (mm)

RSM = Response Surface Methodology

GRA = Grey Relational Analysis

## 1.- Introduction

In recent decades, additive manufacturing has brought a major change in the way the products are manufactured. This technology, also called 3D printing, has changed numerous industrial sectors, including automotive, aerospace, and healthcare, among others (Altıparmak & Xiao, 2021; Ghidini et al., 2023; Guo & Leu, 2013). The design flexibility, the reduction of waste, and the capability of producing complex geometries that are unfeasible with traditional manufacturing methods are currently revolutionizing the manufacturing landscape (Lin et al., 2021).

Among the various additive manufacturing processes, Fused Filament Fabrication (FFF), also known as Fused Deposition Modelling (FDM), is distinguished by its relative simplicity, lower cost and the wide materials range that can be used, making it an attractive option for industrial applications as well as for domestic and educational use (Bahnini et al., 2018; Garcia-Dominguez et al., 2020).

In this context, Nylon is one of the most versatile and prominent materials applied in additive manufacturing using FFF technologies (Fathi & Dickens, 2013; Terekhina et al., 2019). Among its different attributes, this thermoplastic offers a combination of properties that make it ideal for a wide applications range, from functional prototypes to end-use parts in industries such as automotive and aerospace (Martinez et al., 2022). Its high mechanical strength and toughness, high flexibility, good wear resistance, thermal stability and resistance to chemical attack compared to other thermoplastic materials makes it suitable for manufacturing end-use parts (Ketan Vagholkar & Parth Vagholkar, n.d.; Song et al., 2005; Yunus et al., 2005). In particular, nylon is employed in the manufacture of final components that require a combination of lightweight and robust properties, including brackets, housings and structural parts, being its wear resistance and thermal stability ideal for these applications (Moreno-Núñez et al., 2023; O'Connor & Dowling, 2019).

The use of Nylon is increasing in industries such as automotive and aerospace, where producing parts with high geometric accuracy is essential for ensuring the functionality and integration of printed parts into wider components. For example, geometric deviations lead to assembly failures, performance problems and, in extreme cases, a structural failure of the component in service (Braian et al., 2016; Oh et al., 2022; Rupal et al., 2020). Consequently, it is important to perform an exhaustive geometry control that guarantee the required specifications and tolerances (Minetola et al., 2020; J. Singh et al., 2016; Valerga Puerta et al., 2020). In addition to dimensional tolerances, form deviations and surface roughness are attributes of manufactured parts that are of great interest in high value-added industries (Karamimoghadam et al., 2023; Vazquez-Martinez et al., 2020). However, these characteristics of surface finish have not been studied so intensively until nowadays, when the focus of the production using additive technologies has shifted from the manufacturing of prototypes to obtaining final parts (Felbrich et al., 2018; Sharma et al., 2023). This trend has increased the interest of the scientific community in studying not only the properties of 3D-printed parts, but also the process parameters that affect these properties.

The final properties of FFF-produced parts are highly dependent on the precise control on the printing parameters. Factors such as temperature, printing speed, and layer thickness significantly influence the mechanical strength, surface finish, and dimensional accuracy of the printed components (García Plaza et al., 2019a; Kechagias et al., 2022a). Variations in these parameters can lead to deviations in the expected performance and the final part quality. Consequently, it is crucial to consider the process parameters in order to ascertain the final conditions of the part.

One of the most studied variables is temperature. Heat is a requisite for the deposition of layered material by FFF technologies, and represents a crucial parameter, as it is directly related to volume variations that ultimately influence the final geometry of the part (Nahar & Gurrala, 2022; Oskolkov et al., 2021). Another significant parameter is the speed at which the material is deposited on the layer, known as printing speed. From a production standpoint, although increasing the speed reduces manufacturing times (Qin et al., 2019; R et al., 2021), high speeds may result in defects in the final product, such as porosity and high surface roughness, Or equipment vibrations that generate geometric distortions in the part. Layer thickness is also the subject of many studies, as increasing this parameter reduces manufacturing times (Alafaghani & Qattawi, 2018; Yang & Yeh, 2021), although it is also related to a negative impact on the mechanical properties and geometry of the resulting parts (Letcher et al., 2015; Nomani et al.,

2020). Additionally, other parameters such as layer orientation, nozzle diameter and raster orientation have been also studied in the literature for different materials.

The effect of printing speed, layer thickness and build orientation on geometrical deviations was analysed by E. García et al. (García et al., 2020) for PLA-Graphene parts manufactured by FFF. In this study, different parts printed using printing speeds from 20 to 80 mm/s and values of layer thickness from 0.06 to 0.24 mm. The results indicate that the upright orientation achieved the best dimensional accuracy, in contrast with the flat orientation which showed poorest accuracy. Regarding the printing speeds, the authors stated that larger extruder movements increase the errors due to the accumulation of single positioning errors. Nevertheless, the lowest flatness deviation was obtained with flat orientation, achieving the on-edge orientation the higher deviation. In addition, they found that an increase of printing speed and layer thickness, respectively, affects negatively dimensional accuracy of the manufactured parts.

The same three parameters were studied by E. Garcia et al. (García Plaza et al., 2019a) in order to assess their effect on dimensional deviations and flatness in PLA parts produced via FFF. In terms of dimensional deviations, the results shown that none of the three variables studied are significant. However, on-edge orientation demonstrated favourable dimensional outcomes, in any direction at low printing speed and low layer thickness. Conversely, reducing layer thickness was identified as a significant factor that affects flatness positively, reducing the value of the shape deviation.

The effect on surface roughness and dimensional accuracy of different parameters for acrylonitrile butadiene styrene (ABS) parts produced by FFF was studied by S. Vyavahare et al. (Vyavahare et al., 2020). In their study, they analysed layer height, deposition rate, layer orientation, shell thickness and extrusion temperature as input variables. Their initial results showed dimensional deviations ranging between 8.9% and 9.8% of the nominal values. They found that the layer thickness is statistically significant, and that surface roughness (*Ra*) increases with layer thickness. They also found that in terms of dimensional accuracy, the layer thickness proves to be influential, with better results at intermediate values (0.2 mm) than at the extreme values of the range studied (0.1-0.3 mm). Regarding the other variables, no clear influence on dimensional accuracy was observed.

In relation with the nozzle diameter, S. Khatoon et. al. (Khatoon & Ahmad, 2023) analysed the dimensional errors obtained in the fabrication of polymethyl methacrylate micropillars for biomedical applications via FFF were investigated. The nozzle diameter was varied (0.20, 0.25 and 0.30 mm) while the remaining parameters were held constant. The results indicated that the

optimal nozzle diameter for achieving dimensional accuracy was 0.25 mm because is the most suitable choice as it optimizes filament deposition, minimizes thermal defects, improves layer quality, and maintains efficient print times.

In addition to the previously mentioned variables, the filament colour has also been considered in the study of the dimensional accuracy of parts obtained by FFF. As indicated in (Frunzaverde et al., 2023), the thickness of red PLA parts increased by up to 12%, while parts obtained with black filament exhibited a deviation exceeding 5%. In this instance, although a greater discrepancy was observed at higher layer thicknesses (0.2 mm), no discernible trend was evident when varying the value. Authors considered that the colour of the filament significantly affects the dimensional accuracy of 3D-printed PLA parts due to variations in the thermal properties and material flow behaviour caused by pigmentation additives.

Although the above mentioned parameters are related to geometrical properties and surface roughness, there are few studies that analyse the effects of these parameters on parts printed using Nylon. Among these studies, I. Buj-Corral et al. (Buj-Corral & Zayas-Figueras, 2023), performed a comparative analysis to investigate the dimensional error and roundness in the fabrication of a cylindrical spur gear by FFF using PLA and Nylon PA6. For this purpose, different printing temperatures and bed temperatures were set for manufacturing PLA and Nylon gears, respectively, and a unique layer thickness value of 0.2 mm. The results showed that the gear obtained with PLA provided better dimensional accuracy compared to Nylon (0.23% in PLA, 2.30 % in Nylon), with lower relative errors in key measurements, whereas the Nylon gear had better roundness accuracy (0.254 in PLA gear, 0.177 mm in Nylon gear) , which was attributed to differences in infill rates.

A relevant investigation on Nylon was also provided by K. Rashed et. al. (Rashed et al., 2022), who analysed the influence of infill density, layer height, infill pattern and raster orientation in surface roughness and different mechanical properties of pieces obtained by FFF. They stated that the infill density (80-100%) is the sole significant variable influencing surface roughness, as higher infill density contributes to a smoother surface finish in the printed parts. Conversely, large layer thickness was related to elevated surface roughness. However, given the dimensions employed to fabricate the specimens (0.1 and 0.2 mm), this variable is not deemed statistically significant.

Similar outcomes to those reported by S. Vyavahare et al. (Vyavahare et al., 2020) for ABS were obtained by R. Tahir (Mushtaq et al., 2022) in the *Ra* of parts produced by FFF of ABS and Nylon 6. Regarding Nylon, they found that reducing the *Ra* value must be accompanied with a reduction of layer thickness, printing speed, and an increase of temperature.

A review of the literature shows that few studies have investigated the influence of process parameters on the mechanical and surface properties of parts manufactured by FFF (Dobrzańska-Danikiewicz et al., 2023; Durgun & Ertan, 2014; Rajpurohit & Dave, 2019; Ralchev et al., 2021), and Nylon remains a relatively understudied material. Given that this material is increasingly used to produce final parts in high-value manufacturing sectors, it is necessary to study the influence of process parameters on the geometric deviations of final parts in order to optimize the manufacturing process. Accordingly, the present study aims to evaluate the impact of layer thickness, printing speed, and extrusion temperature on the geometry of hollow cylindrical Nylon 12 parts, representing an axis-hole system. This will facilitate the establishment of optimal manufacturing conditions through Grey Relational Analysis (GRA). Although previous studies have explored the influence of process parameters on the dimensional accuracy of FFF parts, very few have focused on Nylon 12 materials. Moreover, most research has either used statistical modelling techniques or direct correlation analyses, but not a combined approach. In this study, a novel methodology is proposed by integrating Response Surface Methodology (RSM) to build predictive models and Grey Relational Analysis (GRA) for multi-response optimization. The RSM models provide predicted values which are subsequently used in GRA, allowing for a more accurate optimization over a broader set of process parameters. This combined approach addresses a gap in the literature and provides a comprehensive understanding of the process–geometry relationship in FFF of Nylon 12 parts.

## 2. Methodology

In order to evaluate the influence of the manufacturing parameters on the geometrical properties of Nylon 12 parts obtained by FFF, a cylindrical-type part has been designed. The hollow cylindrical specimen was designed to evaluate the potential influence of the parameters on a concave or convex surface. This geometry allows to determine whether the effects could be noticeable in a cylindrical part with different radius. Furthermore, the thickness and height of

the specimens were set to provide enough rigidity and stability to be manipulated and measured. The specific dimensions of the specimens are illustrated in Figure 1.

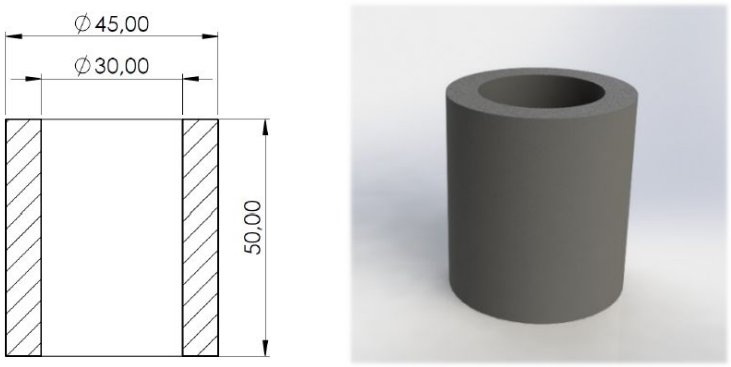


**Figure 1.** Design dimensions (in mm) of the test pieces to be manufactured.

A set of specimens with the design conditions was obtained by means of Fused Filament Fabrication. The specimens were printed using a Raise 3D Pro2 model printer (Figure 2). This equipment has an extrusion capacity up to a maximum temperature of 300 °C and a resolution per layer up to 0.01 mm. The G-code for the printing process was obtained using the slicing software idea Maker.

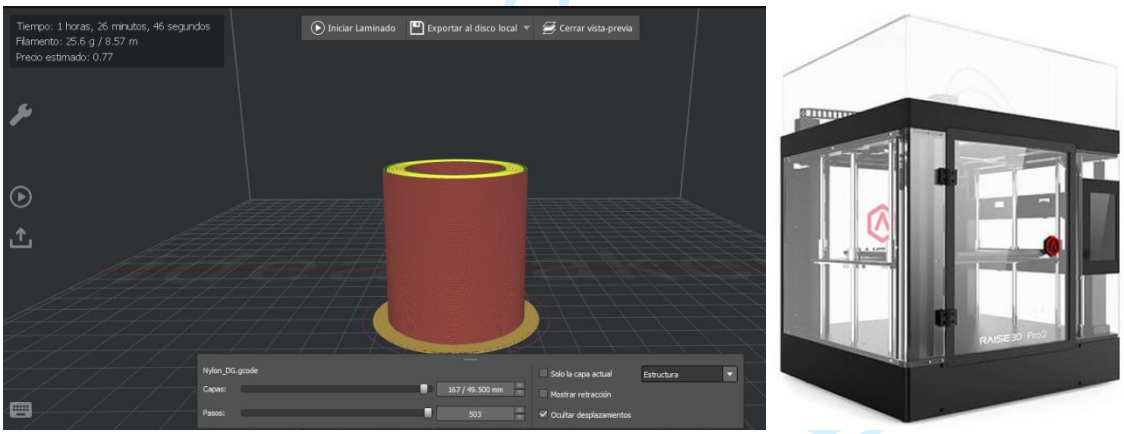


**Figure 2.** Slicing software and equipment used for the test tube fabrication.

To analyse the influence of the manufacturing parameters in the geometrical properties, the printing speed ($v$), the temperature ($T$) and the layer thickness ($e$) have been varied, producing a total of 18 specimens corresponding to the values shown in Table 1.

It must be noted that Nylon printing requires low values of $v$ to ensure the enough quantity of the material during the extrusion process, as reported by R. T. Mushtaq et al. (Mushtaq et al., 2022), whereas the range of temperature selected correspond to the values recommended for filament manufacturer (240 – 270 °C). In addition, $e$ values were selected to maximize the piece resolution, as it is the case of the lowest $e$ value (0.1 mm) and to minimize the manufacturing time, as it is the case of the higher $e$ value (0.3 mm) (Shakeri et al., 2021a).

**Table 1.** Values of the manufacturing parameters variables.

| $v$ (mm/s) | $T$ (°C) | $e$ (mm) |
|---|---|---|
| 40 | 240 | 0.1 |
| | 255 | 0.2 |
| 60 | 270 | 0.3 |

The layers deposition has been carried out in the cylinder generatrix direction (vertical direction). This orientation has been observed to reduce the amount of material used, as no support material is required. Furthermore, previous studies have demonstrated that this orientation exhibits less geometrical errors compared to a horizontal direction (García et al., 2020b; Hooshmand et al., 2021).

The remaining manufacturing parameters have been maintained at a constant level. The specific values are presented in Table 2. To implement these parameters in the production of the parts, IdeaMaker slicing software was employed.

**Table 2.** Printing conditions.

| | |
|---|---|
| Infill density | 100 % |
| Bed temperature | 110 °C |
| Exterior Shell number | 2 |
| Interior Shell number | 2 |

A total of 18 specimens were obtained by considering each of the possible combinations of the previously established values of $v$, $T$ and $e$. The dimensions of the outer diameter ($D_{ou}$), the inner diameter ($D_{in}$) and the height ($H$) of the piece were measured for the geometric control of these specimens.

An outside micrometre was employed to measure the outer diameter $D_{ou}$, performing four diameter measurements for each specimen, located at four different heights in intervals of 10 mm apart. In the case of the $D_{in}$ measurement, a three-contact inside micrometre was used, yielding four measurements at different heights as performed with the outer diameter. All measurements were repeated four times for each specimen and the average value was considered to minimize the influence of measurement variability. For the height, a depth probe was used, resulting in the measurement of $H$ at four different positions at intervals or 90 degrees. Table 3 illustrates the specifications of the instruments utilized for measurement. Prior to data acquisition, the apparatus underwent calibration using longitudinal standard blocks, resulting in an uncertainty value commensurate with the scale division of each instrument.

**Table 3.** Metrology characteristics for dimensional equipment used.

| | Outside micrometre | Three contact Inside micrometre | Depth CALYPER |
|---|---|---|---|
| Model | IROKO D1 1081 | MITUTOYO, MAH2 | RS PRO |
| Scale division (mm) | 0.01 | 0.01 | 0.01 |
| Measuring range (mm) | 0-150 | 25-30 | 0-150 |

A Mitutoyo portable roughness meter, model SURFTEST SJ-210, was employed to ascertain the surface finish. The resulting measurement is indicative of the arithmetic mean roughness (*Ra*). Four *Ra* values were obtained on the outer surface of each specimen, as well as on the inner surface. This was achieved by measuring four generatrixes on the upper part and four generatrixes on the lower part, separated by 90° for each. A Gaussian filter has been used to obtain the roughness profile. The scan length ($l_s$) was 25 µm and the contact length ($l_c$) was 8 mm according to ISO 21920-3:2021 standard (International Organization for Standardization, 2021).

The macrogeometrical deviations were measured for every specimen with a form-measuring machine of ACCRETECH, model RONDCOM NEX (Figure 3). Five roundness (*RON*) measurements were carried out at the inner surface and at the outer surface, respectively, in intervals of 10 mm along the cylinder generatrix. Among the different mathematical methods to obtain the roundness value, according to ISO 12181-1:2011 (International Organization for Standardization, 2011), the least square error method was used, being a common method used in previous researches (Béjar et al., 2019; Bermudo Gamboa et al., 2022). According with the values obtained in each section measured, the circular runout (*CRO*) was obtained.

Regarding longitudinal form deviations, the specimen straightness (*STR*) has been measured for the inner and the outer specimen surface. Along one generatrix, three measurements were carried out separated 5 mm each other and 10 mm length. In addition, the measurements were reproduced in three generatrix, 90º separated each other, obtaining twelve straightness values for each specimen surface. Finally, using the different measurements performed for each specimen, the cylindricity (*CYL*) was calculated.

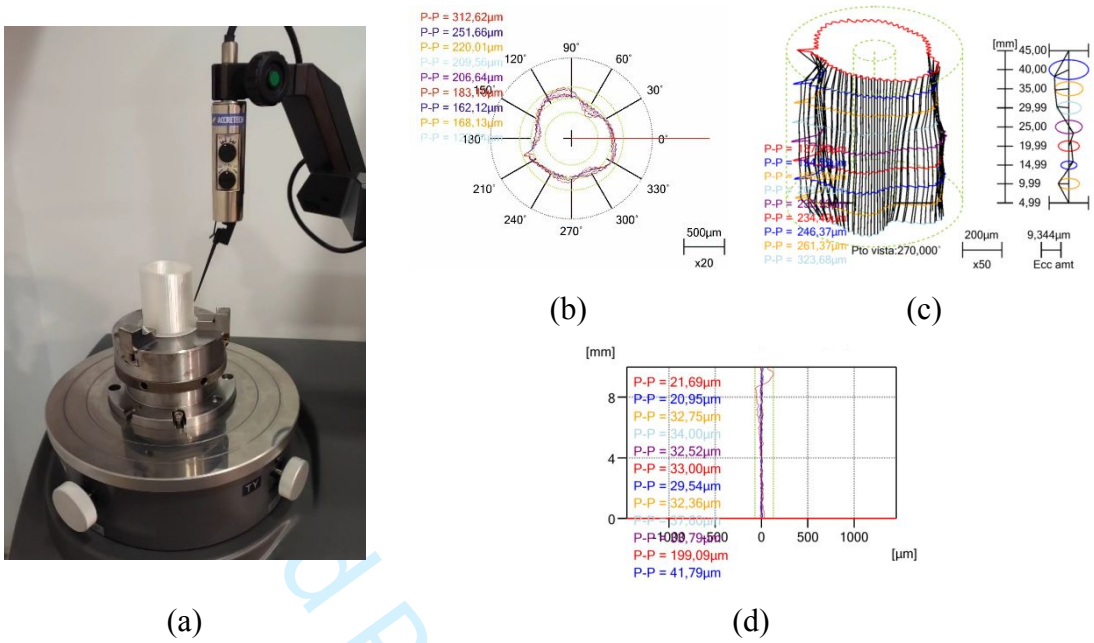


**Figure 3.** Macrogeometrical deviations measurements (a) form-deviations equipment, (b) roundness results, (c) cylindricity results, (d) straightness results.

The experimental results obtained were processed using different analytical techniques to evaluate the influence of manufacturing parameters on the geometric deviations and surface roughness of the printed parts. The relationship between these parameters and the studied variables was analysed using the Pearson correlation coefficient, which allows for a precise evaluation of the linear dependence variables. This method is particularly suitable for identifying trends and quantifying the influence of process parameters on dimensional accuracy.

To develop predictive models and assess the interaction between variables, Response Surface Methodology (RSM) was applied, employing second-order polynomial models. In general, the second-order RSM model is expressed as Equation 1:

$$Y = \beta_0 + \sum_{i=1}^{k} \beta_i X_i + \sum_{i=1}^{k} \beta_{ii} X_i^2 + \sum_{i=1}^{k-1} \sum_{j=i+1}^{k} \beta_{ij} X_i X_j + \varepsilon \quad (1)$$

where $Y$ is the response variable, $X_i$ and $X_j$ are the independent variables, $\beta$ values are the regression coefficients, and $\varepsilon$ is the residual error. In this study, with three independent variables (k=3) corresponding to printing speed ($v$), extrusion temperature ($T$), and layer thickness ($e$), the fitted model takes the form of Equation 2:

$$Y = \beta_0 + \beta_1 v + \beta_1 T + \beta_1 e + \beta_{11} v^2 + \beta_{22} T^2 + \beta_{33} e^2 + \beta_{12} vT + \beta_{13} ve + \beta_{23} Te + \varepsilon \quad (2)$$

The experimental matrix was designed according to a central composite design, and the regression coefficients were calculated from the experimental data. The model adequacy was evaluated through the coefficient of determination ($R^2$).

RSM is widely used in additive manufacturing as it effectively captures nonlinear behaviours, facilitates process optimization, and enables the identification of optimal manufacturing conditions through mathematical modelling (Temiz, 2024; Vanaei et al., 2022).

Additionally, to optimize and evaluate the best printing conditions, Grey Relational Analysis (GRA) was used, considering that all output variables should be minimized to enhance dimensional precision. GRA is particularly advantageous in multi-response optimization, as it normalizes variables of different scales, ranks parameter configurations based on overall performance, and provides a systematic approach to selecting the most favourable process conditions.

Initially, the experimental results were normalized. To do that, it is necessary to take into account if lower or higher results are better. In this case, smaller values of geometrical deviations and surface roughness values are better. Equation 3 was used to normalize the experimental results in both cases.

Smaller is better

$$Z_k = \frac{\max(x_i) - x_k}{\max(x_i) - \min(x_i)} \quad (3)$$

Where different variables correspond with:

- $Z_k$ : Normalized value for the output variable in a cutting parameter combination.
- $x_i$ : Set of output variable values
- $x_k$ : Output variable value in a cutting parameter combination.

Reference value ($R$) has been selected as the maximum value of $Z_k$. Then, the normalized values variations ($\Delta_k$) were calculated (Equation 4).

$$\Delta_k = |Y_k - R| \quad (4)$$

The identificatory coefficient ($\xi_k$) has been calculated according Equation 5. These values are between a 0 to 1 range.

$$\xi_k = \frac{min(\Delta_k) + 0.5 \cdot max(x_k)}{\Delta_k + 0.5 \cdot max(x_k)} \quad (5)$$

Finally, the mean value of the identificatory coefficients corresponds with the GRC values (Equation 6). These results allow to rank the best performing cutting parameters (higher GRC values) against the worst performing combinations (lower GRC values).

$$GRC = \xi_k = \frac{\sum_{k=1}^{n} \xi_k}{n} \quad (6)$$

The use of GRA has been shown to be effective in additive manufacturing studies for selecting the most suitable processing parameters in multi-criteria decision-making environments (Shakeri et al., 2022; M. Singh & Bharti, 2022).

## 3. Results

Once the specimens were obtained for the different combinations of temperature, printing speed and layer thickness, a series of measurements were taken to perform a geometry analysis. The measurement results are presented according to three categories corresponding to each subsection of the results section: dimensional deviations, form deviations and surface roughness. In each case, the influence of the manufacturing parameters on the magnitudes under analysis was investigated. Based on these results, a mathematical model has been proposed to predict each of these magnitudes, respectively, as a function of the manufacturing parameters.

### 3.1. Dimensional Deviations Analysis

Figure 4 illustrates the deviations in the values of the outside and inside diameter and the height of the specimens as a function of the printing speed, the extrusion temperature and the layer thickness.

In general terms, it can be observed that the specimens obtained have a lower value of outer and inner diameters in comparison to their design dimensions. This phenomenon can be attributed to the volumetric contractions during the cooling of the deposited material, and it is inherent to the thermal process necessary for the filament extrusion. With regard to the height of the cylinders, the deviations obtained in comparison to the nominal height are lower than in the case of the diameters. In this case, larger and smaller dimensions than the nominal were observed indistinctively, without a discernible pattern.

The results depicted in Figure 4a, which corresponds to a deposition rate $v$ = 40 mm/s, shown a decrease of the deviation of the outer diameter as the extrusion temperature increases. However, that trend observed for the lowest deposition rate was not observed for the highest deposition rate ($v$ = 60 mm/s), where the maximum reduction of the deviation was obtained for the intermediate temperature $T$ = 255 °C (Figure 4b). It must be noted that the outer diameter deviations are negative independently of the value of the printing parameters, which corresponds with a reduction of the diameter with respect to the nominal.

Furthermore, a reduction of the deviation was observed at the highest extrusion temperature (270 °C) in comparison to the lowest temperature (240 °C). Regarding the influence of layer thickness on the outer diameter, the results show an increase of the deviation with respect to the nominal as the value of this parameter increases, which is irrespective of $T$ and $v$. This is due to the adjustment that is originates in the extruded bead at the ends, which has a different width

due to the thickness of the layer, thereby modifying the final dimension of the part. This result is aligned with previous studies (Elayeb et al., 2024; García Plaza et al., 2019b).

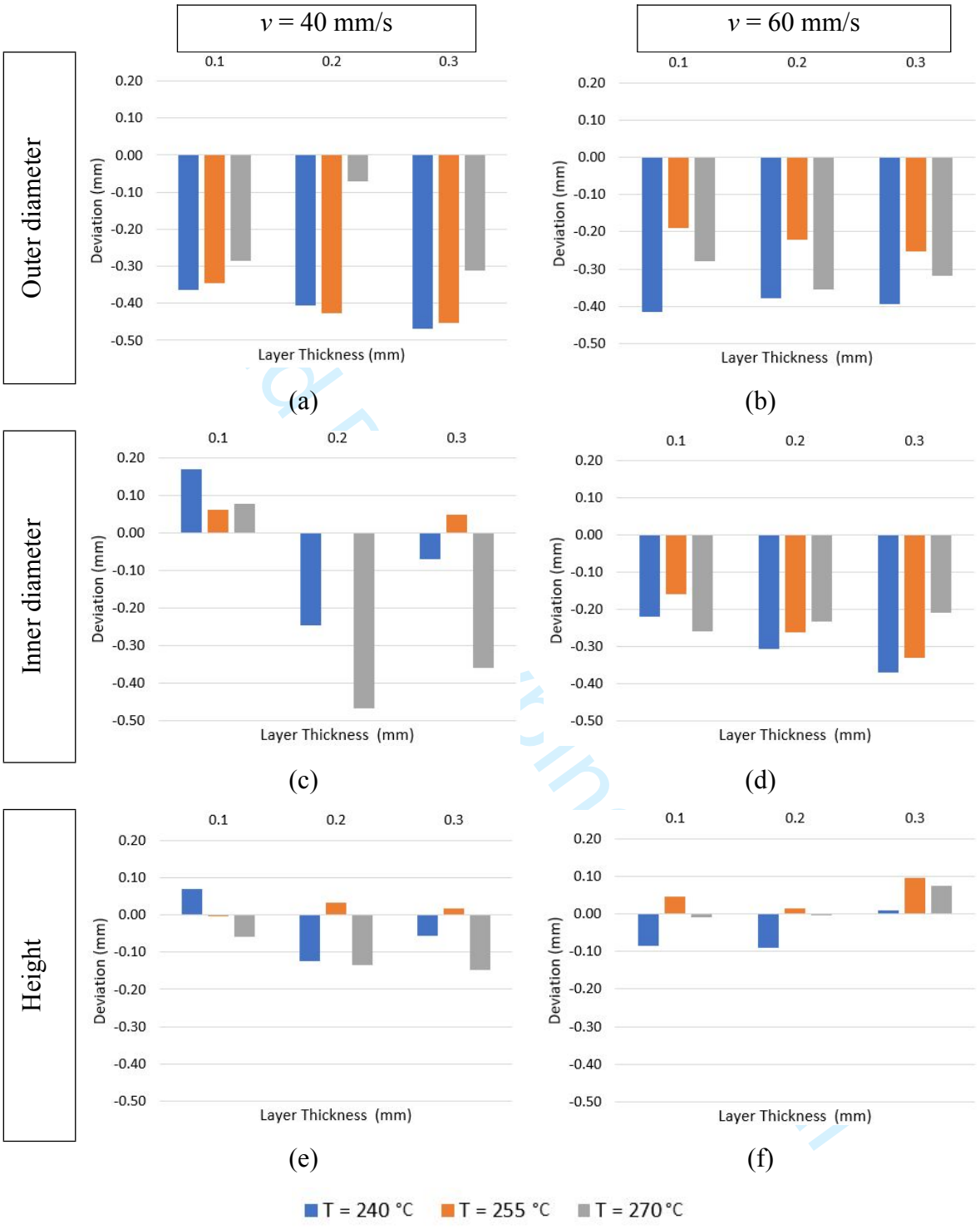


**Figure 4.** Geometrical deviations for different temperatures and layer thickness corresponding to (a) Outer diameter and $v$ = 40 mm/s; (b) Outer diameter and $v$ = 60 mm/s; (c) Inner diameter and $v$ = 40 mm/s; (d) Inner diameter and $v$ = 60 mm/s; (e) Height and $v$ = 40 mm/s; (f) Height and $v$ = 60 mm/s.

Attending to the inner diameter, deviations of different sign were obtained for $v$ = 40 mm/s, as represented in Figure 4c. The deviations were positive for the smallest value of the layer thickness ($e$ = 0.1 mm), while for the other two values they were negative in most of the cases analysed. In this case, the smallest error was obtained for the intermediate temperature. However, for the highest speed value ($v$ = 60 mm/s) represented in Figure 4d, this behaviour is only observed for $e$ = 0.1 mm, while for 0.2 and 0.3 mm the deviation decreases when the temperature increases. It is necessary to consider the temperature values used to carry out the tests, the maximum and minimum values correspond to the extreme values of the material for a correct operation, so at intermediate values the creep capacity of the material in the extruder die could be considered more adequate at these intermediate temperature values.

For the lowest value of $v$, it is not possible to establish a clear influence of $e$ on the deviations obtained. However, for $v$ = 60 mm/s an increase in deflection with increasing $e$ is observed at extrusion temperature values of 240 and 255 °C.

The height is the dimension with the smallest dimensional deviation analysed. This result is due to the better control of the displacement of the printer head along the Z axis, which defines the layer thickness. Furthermore, the layer by layer process causes that any excess of material deposited in a specific layer gets displaced in the following layer, which allows for a best control of the layer height. In contrast, in the XY plane the deviations are mainly affected by the creep of the material and the volumetric contractions due to temperature, which produce the flux of the material during the deposition and its contraction during the cooling process.

Regarding temperature and layer thickness, they did not show a clear influence on the deviation from the nominal part height. However, for $v$ a slight increase can be observed as the speed increases, although this trend could be considered as not very relevant.

With the aim of determining the correlation among the different variables analysed, a Pearson correlation analysis was performed. Table 4 shows the values of the Pearson correlation coefficients of the output variables with respect to the input variables (between the output and the input variables). These results are in line with the experimental results, where a greater significance of the extrusion temperature on the O.D. deviation was observed, with the value of the deviation increasing as the temperature increases. These results of this analysis align with the analysis previously performed in this section, showing (1) a greater influence of the extrusion temperature on the dimensional deviation of the outer diameter than on the inner diameter, and (2) an increase of this deviation with temperature.

In relation to $D_{in}$, a significance is shown in relation to the printing speed, with an inverse relationship in this behaviour, where an increase in $v$ tends to reduce the inner diameter

deviation. However, the relationship between $v$ and $H$ is direct, with higher values of $v$ increasing the value of the deviation.

Among the variables studied, $e$ is the one that has shown the least relevance, with a slight significance in the deviation of the inner diameter.

**Table 4.** Pearson correlation values in the dimensional deviations

| | $D_{ou}$ | $D_{in}$ | H |
|---|---|---|---|
| $v$ | 0.19 | -0.49 | 0.35 |
| $T$ | 0.55 | -0.16 | -0.01 |
| $e$ | -0.22 | -0.34 | 0.04 |

Using the Response Surface Methodology (RSM), second-degree polynomial models were obtained, allowing to relate the deviations from the nominal value of each of the output variables studied with the input variables used in the experimental process (deposition rate, temperature and layer thickness). Related with the dimensional deviations, Equations 1 to 3 expose the mathematical model for the outer diameter ($D_{ou}$), inner diameter ($D_{in}$) and piece height ($H$).

To relate the input variables of the process (deposition rate, temperature and layer thickness) to the output variables, a Response Surface Methodology (RSM) analysis with second-degree polynomial models was used. The corresponding mathematical models for the outer diameter ($D_{ou}$,), inner diameter ($D_{in}$) and piece height ($H$) are described by equation 1, 2 and 3, respectively. Additionally, the degree of fitting of each mathematical model has been expressed by means of the $R^2$ value, which are represented in Table 5. As can be seen, the mathematical model corresponding to the outer diameter $D_{ou}$ has a poor fit in its model, whereas the prediction of the model for the inner diameter $D_{in}$ and the layer height $H$, respectively, are fit enough to relate both variables to the manufacturing parameters used in the process.

$$D_{ou}\ (\text{mm}) = 34.8 + 0{,}0472\ v + 0{,}064\ T - 0{,}09\ e - 0{,}000098\ T^2 - 2{,}98\ e^2 - 0{,}000188\ v \cdot T + 0{,}0132\ v \cdot e + 0{,}0014\ T \cdot e \quad (7)$$

$$D_{in}\ (\text{mm}) = 13.5 - 0{,}1287\ v + 0{,}203\ T - 7{,}21\ e - 0{,}000445\ T^2 + 11{,}73\ e^2 + 0{,}000443\ v \cdot T + 0{,}0348\ v \cdot e - 0{,}0001\ T \cdot e \quad (8)$$

$$H\ (\text{mm}) = 30.79 - 19{,}21 - 0{,}0695\ v + 0{,}1671\ T - 4{,}19\ e\ (\text{mm}) - 0{,}000354\ T^2 + 4{,}69\ e^2 + 0{,}000255\ v \cdot T + 0{,}0349\ v \cdot e + 0{,}00233\ T \cdot e\ (\text{mm}) \quad (9)$$

Table 5 shows the fit of each of the models obtained. As can be seen, $D_{ou}$ has a poor fit in its model. This lower predictive accuracy may be attributed to the high sensitivity of the external diameter to slight geometric imperfections, material shrinkage, or thermal deformation phenomena. Consequently, the proposed model should be considered as an approximate predictive tool, valid within the experimental range of this study. In contrast, the regression

models obtained for $D_{in}$ and $H$ exhibited higher $R^2$ values, reflecting a stronger correlation and a better predictive capability within the studied experimental range.

**Table 5.** Models fit values of the geometrical deviations.

| | $D_{ou}$ | $D_{in}$ | H |
|---|---|---|---|
| $R^2$ | 0.490 | 0.704 | 0.837 |

### 3.2. Microgeometrical deviations analysis

Figure 5 shows the experimental results of the arithmetic mean of the roughness ($Ra$) measurements of each of the specimens obtained for each of the manufacturing conditions used during the experimental phase. These results are shown for both the outer and inner surfaces of the cylinder.

In general, the roughness analysis of the outer and the inner surfaces of the cylinder, $Ra_{in}$ and $Ra_{ou}$, respectively, show values of the same order of magnitude. However, the inner roughness values are slightly higher than those on the outer surface, with an increase of $Ra$ approximately from 1 to 5 µm in the different specimens measured. This difference is probably due to the morphology of the surface, which is concave inside the cylinder and convex outside the specimen.

From the results obtained, a clear influence of the layer thickness can be observed independently of the $T$ and $v$ values. For both the inside and the outside of the cylinder, increasing the layer thickness produces an increase of $Ra$. These results are consistent with those obtained using additive manufacturing by material extrusion with other types of conventionally used materials, such as PLA or ABS (Karamimoghadam et al., 2023; Mushtaq et al., 2022; Vyavahare et al., 2020).

For the lowest value of $v$ (40 mm/s) it can be observed that the increase of temperature produces higher values of $Ra$, being this effect more relevant at the first step of temperature (from 255 to270 °C) than at the second step (from 240 to 255 °C). This phenomenon is more pronounced for lower values of $e$ (0.1 and 0.2 mm), while for values of $e$ = 0.3 mm the variation of $Ra$ is not very significant. However, for the highest value of $v$ (60 mm/s), the highest values of $Ra$ are observed at the intermediate temperature (255 °C) and a higher roughness is obtained at the highest temperature (270 °C) compared to the lowest value studied (240 °C).

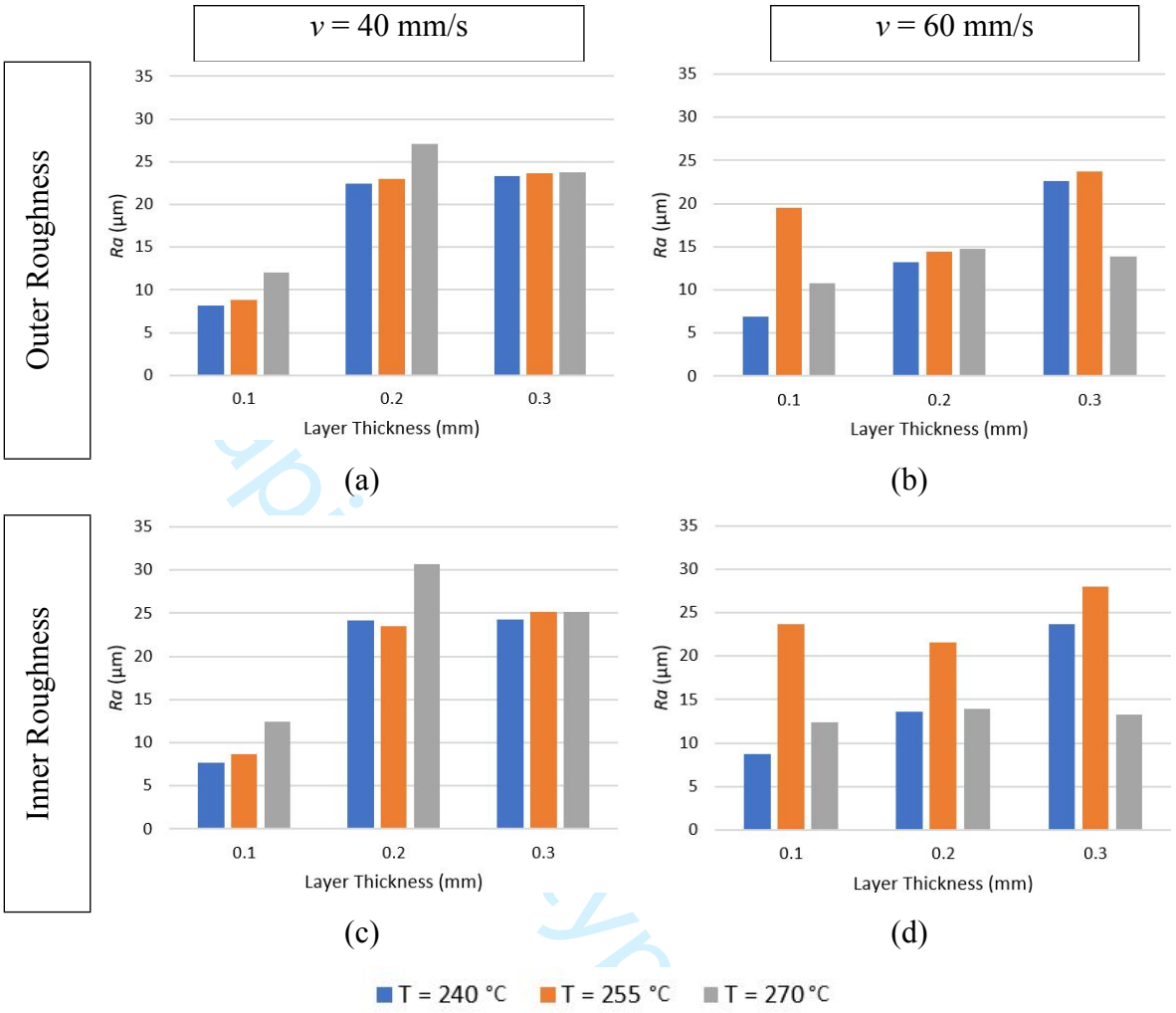


**Figure 5.** Roughness deviation for the different temperature and layer thickness (a) Outer roughness and $v$ = 40 mm/s; (b) Outer roughness and $v$ = 60 mm/s; (c) Inner roughness and $v$ = 40 mm/s; (d) Inner roughness and $v$ = 60 mm/s.

The analysis shows that, on the one hand, the effect of temperature on surface roughness can be related from the thermal contractions and expansions obtained during the manufacturing process. Higher contractions associated with higher temperature values tend to cause surface irregularities that affect negatively the *Ra* value. On the other hand, the increase of $v$ generally leads to reductions in *Ra* up to 40% for a layer thickness of 0.2 mm. This occurs on both the inner and outer surfaces of the samples analysed.

Table 6 shows the Pearson correlation coefficients of the input variables with respect to *Ra* on the outer and inner surfaces, respectively. These results show a significant positive correlation of $e$ with respect to the roughness on both, the inside and outside of the specimen. However, the temperature effect on the manufacturing variables is small, showing only a slight tendency of *Ra* to increase with temperature. This effect can be observed in Figure 5b and 5d, where the *Ra* values for T=255 °C are higher than those at T=270 °C.

With regard to *v*, there is not a high correlation with the *Ra* values obtained, although there is an inverse relationship between the two variables, i.e. an increase of *v* reduces *Ra*.

**Table 6.** Pearson correlation values ion surface roughness.

| | $Ra_{ou}$ | $Ra_{in}$ |
|---|---|---|
| $S_d$ | -0.28 | -0.18 |
| T | 0.06 | 0.05 |
| *e* | 0.69 | 0.62 |

As performed in the previous section for the dimensional deviations, equations 4 and 5 show the models obtained by RSM relating the roughness inside and outside the specimens to the three process variables studied.

$$Ra_{ou}\,(\mu m) = -827 + 1.88\,v + 5.78\,T + 583\,e - 0.0101\,T^2 - 272\,e^2 - 0.00685\,v \cdot T - 1.56\,v \cdot e - 1.34\,T \cdot e \quad (10)$$

$$Ra_{in}\,(\mu m) = -1461 + 2.94\,v + 10.48\,T + 685\,e - 0.0189\,T^2 - 350\,e^2 - 0.0104\,v \cdot T - 2.15\,v \cdot e - 1.50\,T \cdot e \quad (11)$$

The fitting of these models, represented by $R^2$ depicted in Table 7, show a high correlation of the mathematical expressions, therefore allowing to perform accurate predictions about the behaviour of *Ra* for the parameters analysed within the range of study selected. In this regard, the behaviour for the outer surface is slightly better than for the inner surface.

**Table 7.** Models fit values of the inner and outer roughness.

| | $Ra_{ou}$ | $Ra_{in}$ |
|---|---|---|
| $R^2$ | 0.739 | 0.690 |

### 3.3. Macrogeometrical Deviations Analysis

In this section, the geometric deviations of roundness (*RON*), circular runout (*CRO*), cylindricity (*CYL*) and straightness (*STR*) are analysed as a function of the manufacturing parameters. Each of the geometric deviations is evaluated independently by establishing second degree polynomial models from RSM for each of the variables considered. The correlation between each of the analysed macro-geometric deviations and the manufacturing variables considered is then evaluated.

The first shape deviation analysed is *RON*, whose results are shown in Figure 6 for each of the specimens obtained. It can be observed that, given a set of process parameters, the *RON* values obtained are always higher for the outer sections than for the inner sections of the specimens. This result is due to the larger diameter of the outer surface of the cylinder, which caused a greater deviation than that of the inner surface (Kryvyi et al., 2020; Shakeri et al., 2021b).

The increase of *e* produced higher *RON* values in the tests, regardless of the values of *v* and *T*. The greater amount of material deposited, with a greater layer thickness, causes greater *RON*

deviations, especially on the outer and inner faces, where the material can move more freely and therefore produce greater deviations.

With regard to the influence of *v*, it can be considered that the increase in speed has caused an increase in the deviation obtained. This may be due to a greater vibration of the extrusion head, associated with higher speeds, which may cause an increase in the irregularities in the shape of the surfaces obtained (Kechagias et al., 2022b).

With respect to the extrusion temperature, a general trend in the *RON* values with respect to this variable was not observed. However, for the specific case of *e* intermediate values (0.2 mm) and *v* low values (40 mm/s), an increase in temperature caused an increase in the shape deviation, both on the inner and outer surfaces of the part.

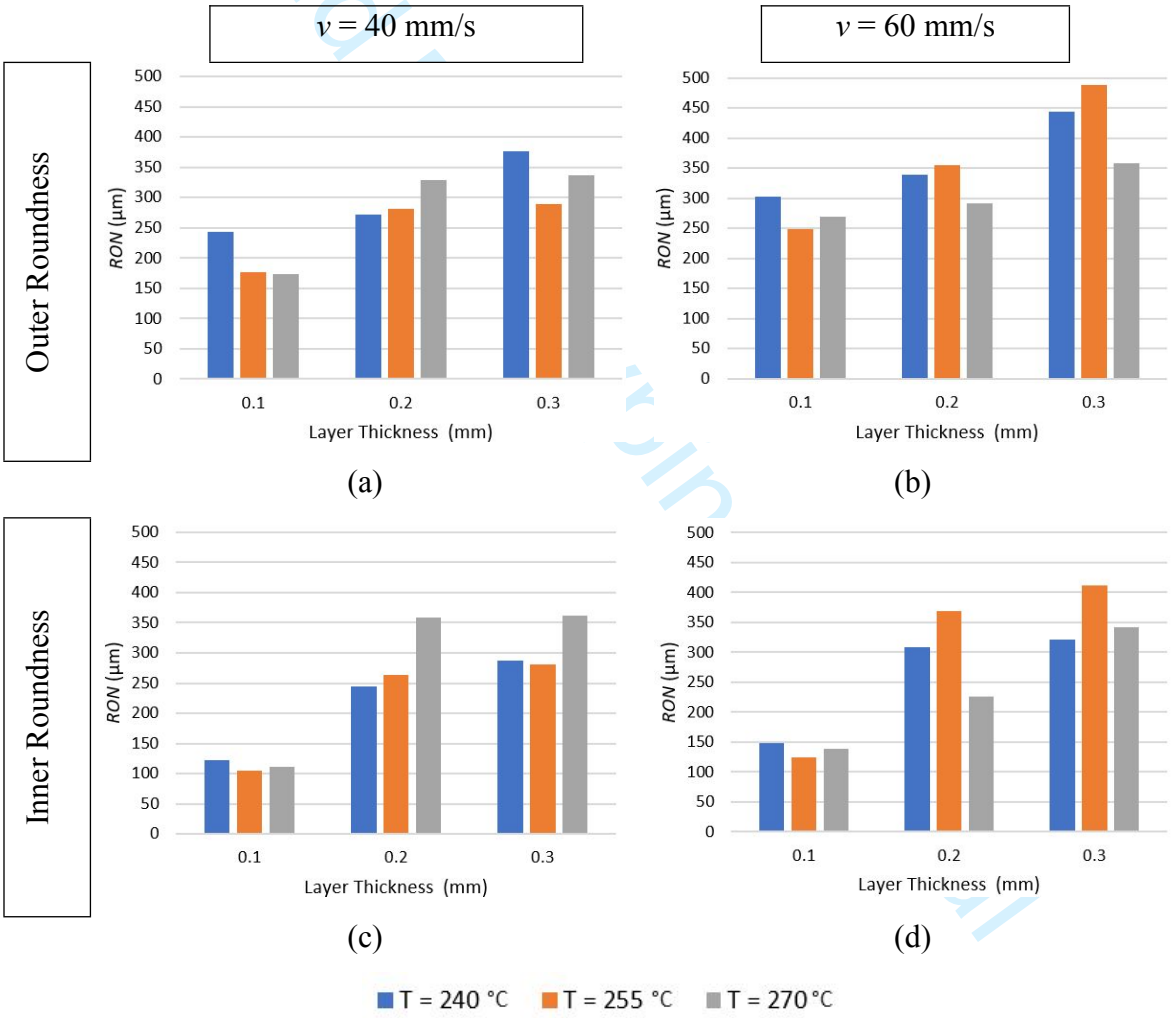


**Figure 6.** Roundness deviation for the different temperature and layer thickness (a) Outer roundness and *v* = 40 mm/s; (b) Outer roundness and *v* = 60 mm/s; (c) Inner roundness and *v* = 40 mm/s; (d) Inner roundness and *v* = 60 mm/s.

As in the case of geometry and surface roughness deviations, second-degree polynomial models have been obtained to relate *RON* to the manufacturing variables used in the production of the part (Equations 6 and 7).

$$RON_{ou}\ (\mu m) = 818 + 18.6\ v - 8.5\ T + 1047\ e + 0.021\ T^2 - 271\ e^2 - 0.0634\ v \cdot T + 5.2\ v \cdot e - 1.8\ T \cdot e \quad (12)$$

$$RON_{in}\ (\mu m) = -4740 + 35.5\ v + 30.2\ T + 879\ e - 0.048\ T^2 - 6532\ e^2 - 0.1382\ v \cdot T + 6.0\ v \cdot e + 9.7\ T \cdot e \quad (13)$$

The fit of the models is shown in Table 8. As can be seen, the results show a good correlation so that these models can be used to evaluate the inner and outer *RON* behaviour over the full range of manufacturing parameters used.

**Table 8.** Models fit values of the inner and outer roundness.

| | $RON_{ou}$ | $RON_{in}$ |
|---|---|---|
| $R^2$ | 0.830 | 0.895 |

The *CRO* values obtained for each of the specimens, both inner and outer, can be seen in Figure 7 as a function of the manufacturing parameters studied ($v$, $T$ and $e$).

In general, it can be observed a slight increase of the values of *CRO* obtained on the inner surface compared to those obtained on the outer surface. This increase is not very significant, except by the results obtained for the specific case of $v$ = 60 mm/s and 0.2 mm layer thickness.

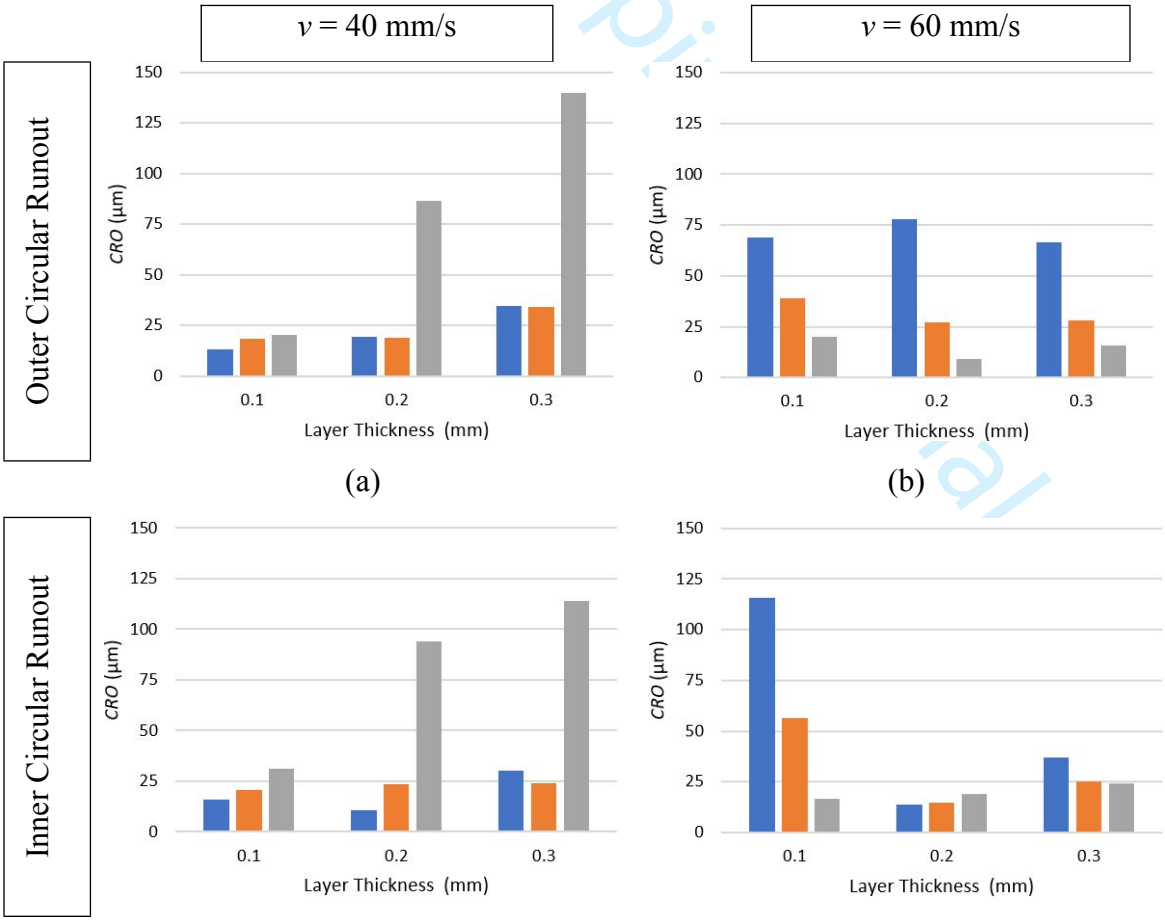

(c) (d)

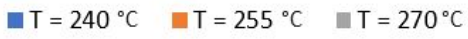


**Figure 7.** Circular runout deviation for the different temperature and layer thickness (a) Outer circular runout and $v$ = 40 mm/s; (b) Outer circular runout and $v$ = 60 mm/s; (c) Inner circular runout and $v$ = 40 mm/s; (d) Inner circular runout and $v$ = 60 mm/s.

Regarding the velocity of the printing head $v$, its influence on *CRO* is not clear for both, the inner and the outer surface, although there is a correlation of $v$ with $T$. At low values of $v$ (40 mm/s), an increase in *CRO* with temperature is observed, while for the highest value of $v$ (60 mm/s) the opposite behaviour takes place. This behaviour can be related to the material creep, as far as at higher temperatures the creep phenomenon increases. Therefore, the combination of creep and high speed produces narrower bead thickness, showing a more regular geometry of the bead, and thus reducing the *CRO* deviation (Quelho de Macedo et al., 2019). This behaviour can also be observed with a combination of low $v$ and low $T$ values, so the correlation between these two variables in terms of this shape deviation is of interest.

In relation with the influence of $e$, it can be noted a greater influence on *CRO* in general than that observed for $v$ and $T$. In this case, for low values of $v$ (40 mm/s), an increase in *CRO* can be observed as $e$ increases. This is due to the fact that a larger amount of deposited material is generated, which has a negative effect on the value of *CRO*. However, the same behaviour cannot be considered for $v$ = 60 mm/s. Although a higher bead height is obtained as $e$ increases, the increase in $v$ tends to produce a narrower bead, which tends to reduce the *CRO* value.

The second order polynomial models for *CRO* both inside and outside the specimens are shown in equations 8 and 9. Table 9 shows the fit obtained in these models, which can be considered a good fit for the range of parameters used in the manufacture of the specimens.

$$CRO_{ou}\ (\mu m) = 3611 + 51.98\ v - 37.4\ T - 1262\ e + 0.0893\ T^2 + 176\ e^2 - 0.1931\ v \cdot T - 14.55\ v \cdot e + 7.98\ T \cdot e \quad (14)$$

$$CRO_{in}\ (\mu m) = 3062 + 44.1\ v - 30.6\ T - 2966\ e + 0.0714\ T^2 + 1342\ e^2 - 0.1604\ v \cdot T - 16.87\ v \cdot e + 12.83\ T \cdot e \quad (15)$$

**Table 9.** Models fit values of the inner and outer roundness.

| | $CRO_{ou}$ | $CRO_{in}$ |
|---|---|---|
| $R^2$ | 0.860 | 0.800 |

The values obtained for the cylindricity of each of the specimens are shown in Figure 8 for each of the values of $v$, $T$ and $e$ used. In this case, lower *CYL* values were obtained on the inside than on the outside of the pieces obtained.

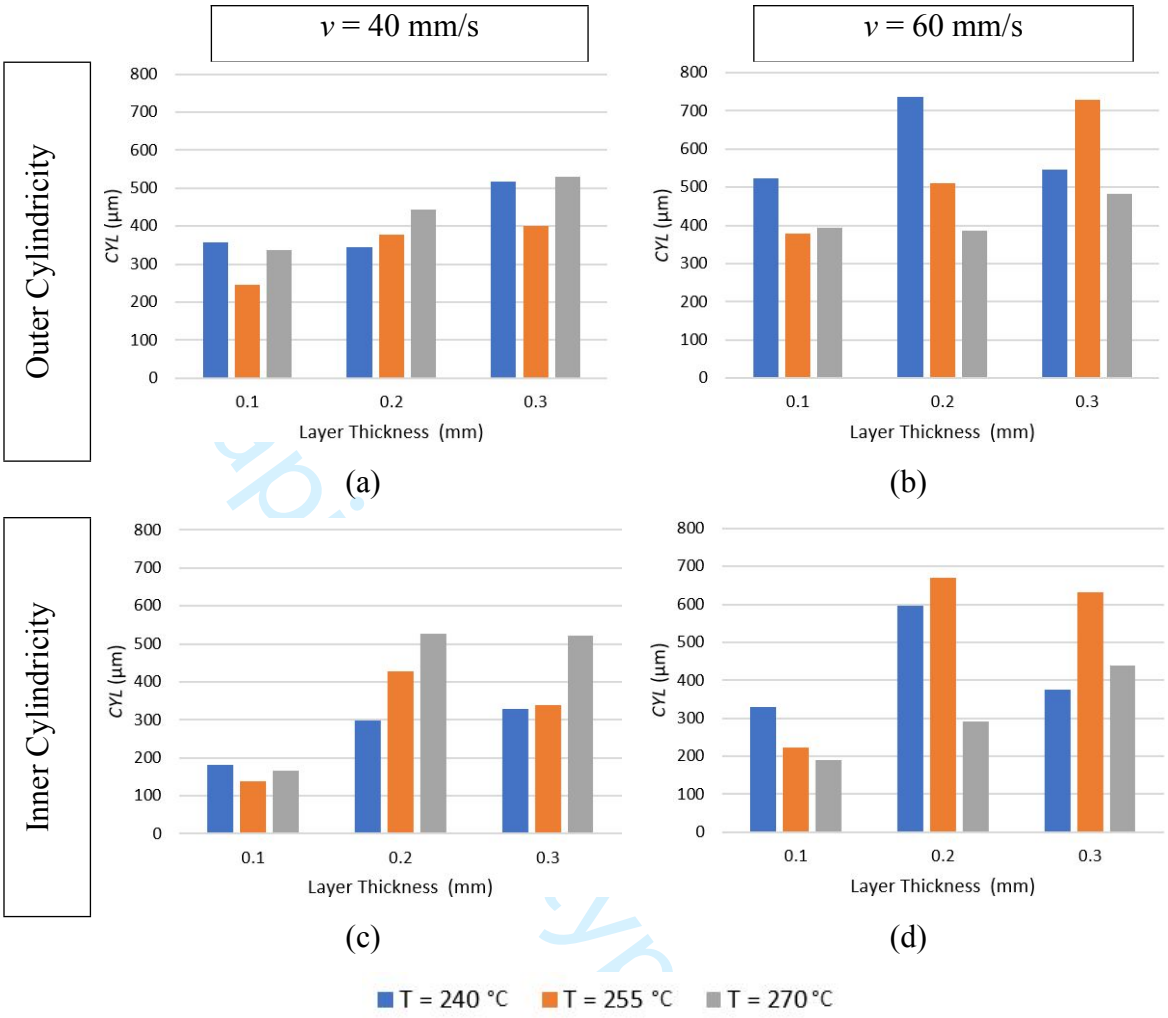


**Figure 8.** Cylindricity deviation for the different temperature and layer thickness (a) Outer cylindricity and $v = 40$ mm/s; (b) Outer cylindricity and $v = 60$ mm/s; (c) Inner cylindricity and $v = 40$ mm/s; (d) Inner cylindricity and $v = 60$ mm/s.

A clear influence of $v$ on $CYL$ values can be observed in the results, independently of $T$ and $e$, with the deviation increasing as the printing speed of the extruded material increases, both inside and outside the part. However, no clear $CYL$ trend can be observed with respect to temperature. Nevertheless, it was observed that high $v$ values (60 mm/s) generate lower CYL values at high temperatures (270 °C) than low values (240 °C).

In terms of layer thickness, there is a clear tendency for the deviation to increase as the $e$ value increases, with this influence being more relevant on the inner surface than on the outer surface. The concavity of the inner surface tends to produce greater irregularities in the shape of the parts obtained, considering a smaller section radius (Shakeri et al., 2021b).

Equations 10 and 11 show the second-degree polynomial models relating the cylindricity deviation to the manufacturing parameters of the sample. The goodness of fit of the models is

shown in Table 10. It can be seen that these models give a good fit over the range of working parameters used.

$$CYL_{ou}\ (\mu m) = 3975 + 97.3\ v - 46\ T - 540\ e + 0.116\ T^2 - 1345\ e^2 - 0.354\ v \cdot T - 4.0\ v \cdot e + 8.2\ T \cdot e \quad (16)$$

$$CYL_{in}\ (\mu m) = -19330 + 115.5\ v + 132\ T - 1701\ e - 0.230\ T^2 - 14629\ e^2 - 0.435\ v \cdot T + 0.1\ v \cdot e \cdot + 34.2\ T \cdot e \quad (17)$$

**Table 10.** Models fit values of the inner and outer cylindricity.

| | $CYL_{ou}$ | $CYL_{in}$ |
|---|---|---|
| $R^2$ | 0.726 | 0.798 |

The last variable measured was straightness on the inside and outside of the cylindrical part. On this occasion, higher deflection values were obtained on the inside than on the outside, with a behaviour similar to that of *CRO*.

Regardless of *T* and *e*, an increase in *v* must result in a reduction in straightness deviation. This improvement in the *STR* deviation is much more sensitive to high values of *T* than to low values. Regarding the influence of *T*, at low values of *v* (40 mm/s), a clear increase in *STR* is observed as *T* increases. On the other hand, at high values of *v* (60 mm/s), the highest values of *STR* are observed at intermediate values of *T* (255 °C).

Finally, an increase in *e* also tends to generate a higher *STR* value, which can be explained by considering the higher surface irregularities associated with the higher *e* values, as observed in the surface roughness (Marcel Kuruc, 2024).

In equations 12 and 13 the polynomial models relating *STR* to the manufacturing variables used in the production of the parts have been presented. The fit of these models is shown in Table 11. Although their fit is inferior to that obtained with the other models, they can be considered adequate ($R^2 > 0.63$) for predicting *STR* values for other values of *v*, *T* and *e*.

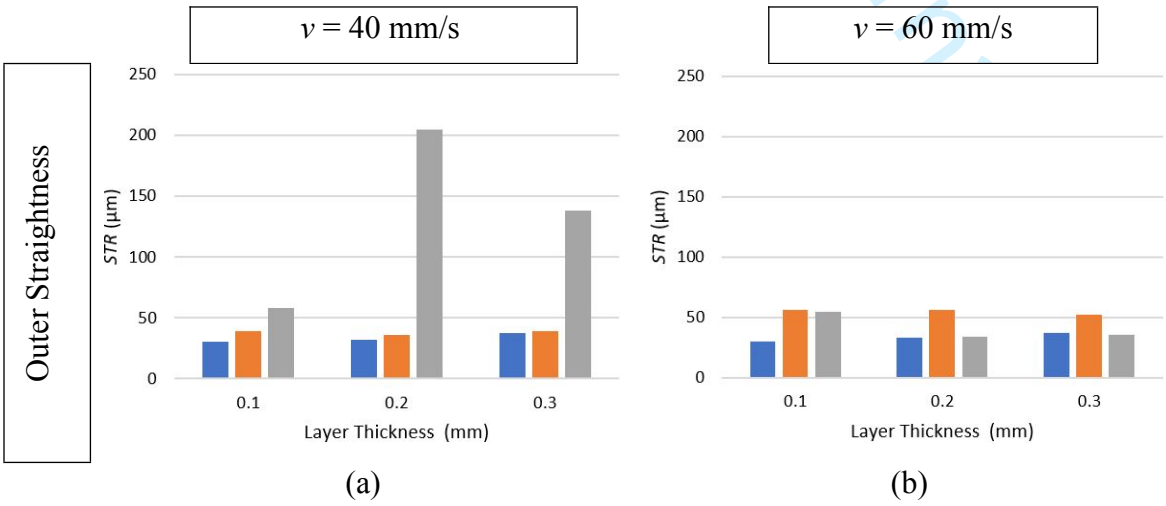


(a) (b)

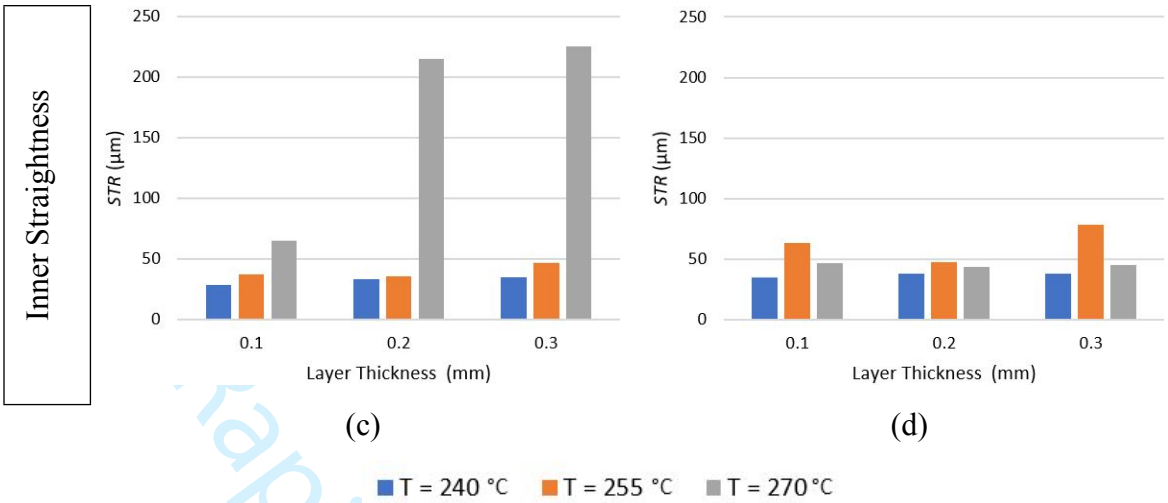


**Figure 9.** Straightness deviation for the different temperature and layer thickness (a) Outer straightness and $v$ = 40 mm/s; (b) Outer straightness and $v$ = 60 mm/s; (c) Inner straightness and $v$ = 40 mm/s; (d) Inner straightness and $v$ = 60 mm/s.

$$STR_{ou}\ (\mu m) = 1720 + 39.8\ v - 22.6\ T + 116\ e + 0.0614\ T^2 - 1525\ e^2 - 0.1542\ v \cdot T - 8.7\ v \cdot e + 3.87\ T \cdot e \quad (18)$$

$$STR_{in}\ (\mu m) = 2803 + 55.5\ v - 33.0\ T - 2067\ e + 0.0855\ T^2 - 689\ e^2 - 0.2133\ v \cdot T - 13.3\ v \cdot e + 12.43\ T \cdot e \quad (19)$$

**Table 11.** Models fit values of the inner and outer straightness.

| | $STR_{ou}$ | $STR_{in}$ |
|---|---|---|
| $R^2$ | 0.631 | 0.735 |

Considering all the deviations analysed, it can be appreciated that there is a relationship in the behaviour depending on the variables used to manufacture the parts ($v$, $T$ and $e$). To facilitate the analysis of the relationship between the deviations, the Pearson correlation coefficients of each of the manufacturing variables with each of the shape deviations have been determined (Table 12).

On the one hand, a similar behaviour of *CRO* and *STR* is observed for the combination of parameters used, especially for low values of $v$ (40 mm/s). Moreover, in both cases it was observed that there is a direct relationship between $T$ and $e$ and the deflections, both inner and outer, whereas for $v$ this relationship is inverse. However, despite a similar correlation, the influence of the manufacturing parameters is greater for *CRO* than for *STR*.

On the other hand, *RON* and *CYL* also show a similar behaviour with respect to the variation of $v$, $T$ and $e$, both on the inner and outer surface of the sample. In this case, $v$ shows a direct correlation with both shape deviations, contrary to the inverse relationship obtained for *CRO* and *STR*. Furthermore, for both deviations, a variation in the way $T$ affects the inside and outside is observed, being inverse for the outside and direct for the inside. This behaviour could be due

to the low significance obtained with respect to the *T* values analysed. Regardless of these correlations analysed, *e* is the most significant variable among those analysed, having a direct relationship with *RON* and *CYL*.

**Table 12.** Pearson correlation coefficients in the form deviations.

| | $RON_{ou}$ | $RON_{in}$ | $CRO_{ou}$ | $CRO_{in}$ | $CYL_e$ | $CYL_i$ | $STR_e$ | $STR_i$ |
|---|---|---|---|---|---|---|---|---|
| *v* | 0.44 | 0.14 | -0.05 | -0.07 | 0.5 | 0.28 | -0.29 | -0.28 |
| *T* | -0.19 | 0.07 | 0.02 | 0.16 | -0.25 | 0.01 | 0.51 | 0.52 |
| *e* | 0.77 | 0.85 | 0.29 | 0 | 0.53 | 0.6 | 0.11 | 0.23 |

### 3.4. Manufacturing parameter optimization

From the set of results obtained in the experimental phase, a grey relational analysis (GRA) was carried out in order to determine the most suitable manufacturing parameters for the production of the parts, based on the different deviations obtained, both at the dimensional level and at the macrogeometric and microgeometric levels.

Table 13 shows the GRC values obtained considering the manufacturing conditions and the corresponding values of each output variable, which have been ranked according to the best conditions obtained in the relational analysis.

The best behaviour was obtained for a low printing speed (40 mm/s), a low layer thickness (0.1 mm) and an intermediate temperature (255 °C) in the range of values suitable for the material extrusion. From the set of results obtained, the lowest value of *e* gives the best results, regardless of the values of *v* and *T*. This fact is related to the high correlation that this variable has with the deviations studied, especially with the macro and microgeometric deviations.

In general, the influence of *v* and *T* is not as clear as that of *e*. However, it can be stablished that regardless of the best conditions obtained, low temperature values (240 °C) and high speeds (60 mm/s) generate greater deviations in the parts produced by FFF.

The results presented above are related to the outer and the inner surfaces together. However, given that the geometry of the part has two different morphologies(shaft-hole), a similar study has been carried out considering a concave and a convex surface independently, so two relational analyses were obtained.

**Table 13.** Manufacturing parameter ranking for the geometrical deviations optimization of the axis-hole piece.

| *v* (mm/s) | *T* (°C) | *e* (mm) | GRC | Rank |
|---|---|---|---|---|
| 40 | 255 | 0.1 | 0.884 | 1 |
| 40 | 240 | 0.1 | 0.815 | 2 |
| 40 | 270 | 0.1 | 0.737 | 3 |
| 60 | 270 | 0.1 | 0.729 | 4 |
| 60 | 270 | 0.2 | 0.708 | 5 |

| | | | | |
|---|---|---|---|---|
| 60 | 240 | 0.1 | 0.692 | 6 |
| 40 | 255 | 0.2 | 0.643 | 7 |
| 60 | 270 | 0.3 | 0.634 | 8 |
| 60 | 255 | 0.1 | 0.634 | 9 |
| 40 | 255 | 0.3 | 0.618 | 10 |
| 40 | 240 | 0.2 | 0.618 | 11 |
| 60 | 255 | 0.2 | 0.604 | 12 |
| 60 | 240 | 0.2 | 0.598 | 13 |
| 40 | 240 | 0.3 | 0.582 | 14 |
| 60 | 240 | 0.3 | 0.555 | 15 |
| 60 | 255 | 0.3 | 0.488 | 16 |
| 40 | 270 | 0.2 | 0.425 | 17 |
| 40 | 270 | 0.3 | 0.400 | 18 |

Table 14 contains the results obtained for the non-coupled analysis of the outer and inner surfaces of the piece, respectively. In addition, the coupled rank has been added to the table to facilitate the comparison. Attending to these results, the best manufacturing conditions coincide with the best case obtained in table 13 for the part as a whole. Nevertheless, the temperature is less relevant in the case of the shaft than for the hole, whereas the speed has better behaviour at low values in both cases.

**Table 14.** Manufacturing parameter ranking for the geometrical deviations optimization of the axis and the hole.

| Shaft | | | | | | Hole | | | | |
|---|---|---|---|---|---|---|---|---|---|---|
| *v* (mm/s) | *T* (°C) | *e* (mm) | GRC | Rank | *Coup. Rank* | *v* (mm/s) | *T* (°C) | *e* (mm) | GRC | Rank |
| 40 | 255 | 0.1 | 0.835 | 1 | 1 | 40 | 255 | 0.1 | 0.917 | 1 |
| 40 | 240 | 0.1 | 0.778 | 2 | 2 | 40 | 240 | 0.1 | 0.893 | 2 |
| 40 | 270 | 0.1 | 0.727 | 3 | 3 | 40 | 270 | 0.1 | 0.772 | 3 |
| 60 | 240 | 0.1 | 0.701 | 4 | 6 | 60 | 270 | 0.1 | 0.746 | 4 |
| 60 | 270 | 0.2 | 0.684 | 5 | 5 | 60 | 240 | 0.1 | 0.715 | 5 |
| 60 | 270 | 0.1 | 0.683 | 6 | 4 | 60 | 270 | 0.2 | 0.690 | 6 |
| 60 | 270 | 0.3 | 0.649 | 7 | 8 | 40 | 255 | 0.2 | 0.662 | 7 |
| 40 | 240 | 0.2 | 0.629 | 8 | 11 | 60 | 240 | 0.2 | 0.646 | 8 |
| 60 | 255 | 0.1 | 0.623 | 9 | 9 | 60 | 255 | 0.1 | 0.645 | 9 |
| 40 | 255 | 0.2 | 0.612 | 10 | 7 | 40 | 240 | 0.2 | 0.641 | 10 |
| 60 | 255 | 0.2 | 0.607 | 11 | 12 | 60 | 270 | 0.3 | 0.639 | 11 |
| 40 | 255 | 0.3 | 0.573 | 12 | 10 | 40 | 240 | 0.3 | 0.629 | 12 |
| 60 | 240 | 0.2 | 0.571 | 13 | 13 | 40 | 255 | 0.3 | 0.629 | 13 |
| 40 | 240 | 0.3 | 0.535 | 14 | 14 | 60 | 255 | 0.2 | 0.561 | 14 |
| 60 | 255 | 0.3 | 0.512 | 15 | 16 | 60 | 240 | 0.3 | 0.551 | 15 |
| 60 | 240 | 0.3 | 0.506 | 16 | 15 | 60 | 255 | 0.3 | 0.471 | 16 |
| 40 | 270 | 0.2 | 0.502 | 17 | 17 | 40 | 270 | 0.3 | 0.379 | 17 |
| 40 | 270 | 0.3 | 0.430 | 18 | 18 | 40 | 270 | 0.2 | 0.359 | 18 |

In summary, the results presented in this section have shown the correlation between different process parameters and a set of output variables. The information obtained from the test has

been processed obtaining mathematical models that can be used to perform geometry predictions. From a technological point of view, one of the main objectives of the industry is the reduction of manufacturing times. In this regards, *v* and *e* are two variables that have a direct influence with the manufacturing time in FFF, as far as the total manufacturing time may be reduced considerably by reducing the layer thickness and/or by increasing the velocity of the printing head. The results obtained indicate that, in order minimize the manufacturing time by increasing the layer thickness, the extrusion temperature must be set as high as possible within the appropriate range for the material extrusion.

## 4. Conclusions

The aim of this work is to analyse the influence of a set of manufacturing parameters, including printing speed, extrusion temperature and layer thickness, on the dimensional, macrogeometric and microgeometric deviations of cylindrical geometry specimens obtained using additive manufacturing processes by material extrusion.

Regarding the dimensional deviations, the specimens manufactured had lower outer and inner diameter with respect to their design values regardless of the set of process parameters selected. The cause of this phenomenon is the volumetric contractions during the cooling of the deposited material after the extrusion of the filament. The height of the cylinders showed smaller deviations compared to the diameters which is consequence of the better control of the process along the Z axis. On contrary, the deviations on the XY plane are more significant due to (1) the lower precision of the printer in the horizontal axes due to dynamic effects of the belts, and (2) the creeping of the material and the volumetric contractions.

The surface roughness analysis showed that both the outer and inner surfaces of the cylinder had similar arithmetic mean roughness (*Ra*) values, with values on the inner surface slightly higher due to its smaller diameter and the concavity. Layer thickness had a notably effect on roughness, with *Ra* increasing with the layer height. This result is consistent with previous studies for other materials such as PLA and ABS. Regarding the extrusion temperature, it also showed a tendency to increase Ra, especially at high values (255-270 °C), which was more pronounced at low layer thicknesses. The deposition rate, on the other hand, showed a significant influence on the reduction of *Ra*, with a decrease of up to 40%.

The analysed shape deviations (*RON*, *CRO*, *CYL* and *STR*) showed different behaviour depending on the manufacturing parameters. In general, higher deposition rates and layer thicknesses increase the deviations value. On the other hand, the extrusion temperature showed lower influence on the deviations with one exception corresponding to the *STR*.

The circularity (*CRO*) and straightness (*STR*) deviations showed an inverse correlation with the deposition rate, with higher printing speed values reducing the deviations. In contrast, cylindricity (*CYL*) and roundness (*RON*) showed a clear tendency to increase with deposition rate, independent of temperature and layer thickness.

In general, it can be said that the layer thickness was the variable with the greatest influence on the values of the geometric characteristics analysed, both at the dimensional level and at the macro and microgeometric level. Lower values of the layer thickness have shown better geometric characteristics in the parts obtained; however, it must be considered that small thickness height considerably increase the manufacturing time. In this regard, the results obtained from the experimental campaign allow to determine the optimal process parameters that must be selected to obtain the tolerances established in the design phase of the parts.

Additionally, to evaluate the deviations in the whole range of the manufacturing parameters, second-degree polynomial models have been obtained using the response surface methodology. These models allow to predict the deviations for a given set of manufacturing parameters. These models will help the industry to optimise the process and improve the quality of the parts produced.

From a technological approach, and attending to the GRA analysis carried out, the smallest deviations were obtained at low rate (40 mm/s) intermediate temperature (255 °C) and low layer thickness (0.1 mm). However, if the resulting parts does not require excessively narrow tolerances, it is convenient to select the highest values of $e$ and $v$ in order to reduce the production time, together with the highest $T$ values.

It is important to highlight that, given the high number of variables that can be evaluated regarding the geometric characteristics of a part obtained through a manufacturing process, the optimization carried out has demonstrated the best manufacturing conditions for producing parts. These results can be directly applied to the components production.

**Fundings**

This work has not received fundings

**Acknowledge**

The authors thank the University of Malaga-Andalucia Tech Campus for its contribution to this work.

**Declaration of competing interest.**

The authors declare that they have no known competing financial interests or personal relationships that could have appeared to influence the work reported in this paper.

**References**

Alafaghani, A., & Qattawi, A. (2018). Investigating the effect of fused deposition modeling processing parameters using Taguchi design of experiment method. *Journal of Manufacturing Processes*, *36*, 164–174. https://doi.org/10.1016/j.jmapro.2018.09.025

Altıparmak, S. C., & Xiao, B. (2021). A market assessment of additive manufacturing potential for the aerospace industry. In *Journal of Manufacturing Processes* (Vol. 68, pp. 728–738). Elsevier Ltd. https://doi.org/10.1016/j.jmapro.2021.05.072

Bahnini, I., Rivette, M., Rechia, A., Siadat, A., & Elmesbahi, A. (2018). Additive manufacturing technology: the status, applications, and prospects. *International Journal of Advanced Manufacturing Technology*, *97*(1–4), 147–161. https://doi.org/10.1007/s00170-018-1932-y

Béjar, S. M., Vilches, F. J. T., Gamboa, C. B., & Hurtado, L. S. (2019). Parametric analysis of macro-geometrical deviations in dry turning of UNS A97075 (Al-Zn) alloy. *Metals*, *9*(11). https://doi.org/10.3390/met9111141

Bermudo Gamboa, C., Martín Béjar, S., Trujillo Vilches, F. J., & Sevilla Hurtado, L. (2022). Geometrical analysis in material extrusion process with polylactic acid (PLA)+carbon fiber. *Rapid Prototyping Journal*, *29*(11), 21–39. https://doi.org/10.1108/RPJ-09-2022-0294

Braian, M., Jimbo, R., & Wennerberg, A. (2016). Production tolerance of additive manufactured polymeric objects for clinical applications. *Dental Materials*, *32*(7), 853–861. https://doi.org/10.1016/j.dental.2016.03.020

Buj-Corral, I., & Zayas-Figueras, E. E. (2023). Comparative study about dimensional accuracy and form errors of FFF printed spur gears using PLA and Nylon. *Polymer Testing*, *117*. https://doi.org/10.1016/j.polymertesting.2022.107862

Dobrzańska-Danikiewicz, A. D., Siwczyk, B., Bączyk, A., & Romankiewicz, A. (2023). Mechanical properties of recycled PLA and PETG printed by FDM/FFM method. *Journal of Achievements in Materials and Manufacturing Engineering*, *119*(2), 49–59. https://doi.org/10.5604/01.3001.0053.9490

Durgun, I., & Ertan, R. (2014). Experimental investigation of FDM process for improvement of mechanical properties and production cost. *Rapid Prototyping Journal*, *20*(3), 228–235. https://doi.org/10.1108/RPJ-10-2012-0091

Elayeb, A., Tlija, M., Eltaief, A., Louhichi, B., & Zemzemi, F. (2024). Minimizing Dimensional Defects in FFF Using a Novel Adaptive Slicing Method Based on Local Shape Complexity. *Journal of Manufacturing and Materials Processing*, *8*(2), 59. https://doi.org/10.3390/jmmp8020059

Fathi, S., & Dickens, P. (2013). Challenges in drop-on-drop deposition of reactive molten nylon materials for additive manufacturing. *Journal of Materials Processing Technology*, *213*(1), 84–93. https://doi.org/10.1016/j.jmatprotec.2012.08.006

Felbrich, B., Wulle, F., Allgaier, C., Menges, A., Verl, A., Wurst, K. H., & Nebelsick, J. H. (2018). A novel rapid additive manufacturing concept for architectural composite shell construction inspired by the shell formation in land snails. *Bioinspiration and Biomimetics*, *13*(2). https://doi.org/10.1088/1748-3190/aaa50d

Frunzaverde, D., Cojocaru, V., Bacescu, N., Ciubotariu, C. R., Miclosina, C. O., Turiac, R. R., & Marginean, G. (2023). The Influence of the Layer Height and the Filament Color on the Dimensional Accuracy and the Tensile Strength of FDM-Printed PLA Specimens. *Polymers*, *15*(10). https://doi.org/10.3390/polym15102377

García, E., Núñez, P. J., Chacón, J. M., Caminero, M. A., & Kamarthi, S. (2020a). Comparative study of geometric properties of unreinforced PLA and PLA-Graphene composite materials applied to additive manufacturing using FFF technology. *Polymer Testing*, *91*. https://doi.org/10.1016/j.polymertesting.2020.106860

García, E., Núñez, P. J., Chacón, J. M., Caminero, M. A., & Kamarthi, S. (2020b). Comparative study of geometric properties of unreinforced PLA and PLA-Graphene

composite materials applied to additive manufacturing using FFF technology. *Polymer Testing*, *91*, 106860. https://doi.org/10.1016/j.polymertesting.2020.106860

García Plaza, E., Núñez López, P., Caminero Torija, M., & Chacón Muñoz, J. (2019a). Analysis of PLA Geometric Properties Processed by FFF Additive Manufacturing: Effects of Process Parameters and Plate-Extruder Precision Motion. *Polymers*, *11*(10), 1581. https://doi.org/10.3390/polym11101581

García Plaza, E., Núñez López, P., Caminero Torija, M., & Chacón Muñoz, J. (2019b). Analysis of PLA Geometric Properties Processed by FFF Additive Manufacturing: Effects of Process Parameters and Plate-Extruder Precision Motion. *Polymers*, *11*(10), 1581. https://doi.org/10.3390/polym11101581

Garcia-Dominguez, A., Claver, J., Camacho, A. M., & Sebastian, M. A. (2020). Analysis of General and Specific Standardization Developments in Additive Manufacturing from a Materials and Technological Approach. *IEEE Access*, *8*, 125056–125075. https://doi.org/10.1109/ACCESS.2020.3005021

Ghidini, T., Grasso, M., Gumpinger, J., Makaya, A., & Colosimo, B. M. (2023). Additive manufacturing in the new space economy: Current achievements and future perspectives. In *Progress in Aerospace Sciences* (Vol. 142). Elsevier Ltd. https://doi.org/10.1016/j.paerosci.2023.100959

Guo, N., & Leu, M. C. (2013). Additive manufacturing: Technology, applications and research needs. In *Frontiers of Mechanical Engineering* (Vol. 8, Issue 3, pp. 215–243). https://doi.org/10.1007/s11465-013-0248-8

Hooshmand, M. J., Mansour, S., & Dehghanian, A. (2021). Optimization of build orientation in FFF using response surface methodology and posterior-based method. *Rapid Prototyping Journal*, *27*(5), 967–994. https://doi.org/10.1108/RPJ-07-2020-0162

International Organization for Standardization. (2011). *ISO 12181-1:2011, Geometrical Product Specifications (GPS) – Roundness – Part 1: Terms, Definitions and Parameters of Roundness*.

International Organization for Standardization. (2021). *ISO 21920-3:2021. Geometrical product specifications (GPS) -- Surface texture: Profile -- Part 3: Specification operators.*

Karamimoghadam, M., Dezaki, M. L., Zolfagharian, A., & Bodaghi, M. (2023). Influence of post-processing CO2 laser cutting and FFF 3D printing parameters on the surface morphology of PLAs: Statistical modelling and RSM optimisation. *International Journal of Lightweight Materials and Manufacture*, *6*(2), 285–295. https://doi.org/10.1016/j.ijlmm.2023.01.004

Kechagias, J., Chaidas, D., Vidakis, N., Salonitis, K., & Vaxevanidis, N. M. (2022a). Key parameters controlling surface quality and dimensional accuracy: a critical review of FFF process. *Materials and Manufacturing Processes*, *37*(9), 963–984. https://doi.org/10.1080/10426914.2022.2032144

Kechagias, J., Chaidas, D., Vidakis, N., Salonitis, K., & Vaxevanidis, N. M. (2022b). Key parameters controlling surface quality and dimensional accuracy: a critical review of FFF process. *Materials and Manufacturing Processes*, *37*(9), 963–984. https://doi.org/10.1080/10426914.2022.2032144

Ketan Vagholkar, P., & Parth Vagholkar, C. K. (n.d.). *Nylon (Chemistry, Properties and Uses) Original Research Paper Nylon (Chemistry, Properties and Uses)*. https://www.researchgate.net/publication/310951621

Khatoon, S., & Ahmad, G. (2023). Rapid prototyping of 3d printed micropillars using fused filament fabrication technique for biomedical applications. *Rapid Prototyping Journal*, *29*(10), 2272–2284. https://doi.org/10.1108/RPJ-03-2023-0096

Kryvyi, P., Dzyura, V., Maruschak, P., Panin, S., Lyashuk, O., & Vlasov, I. (2020). Influence of Curvature and Cross-sectional Shape of Cylindrical Surface Formed by Turning on Its

Roughness. *Arabian Journal for Science and Engineering*, *45*(7), 5615–5622. https://doi.org/10.1007/s13369-020-04512-8

Letcher, T., Rankouhi, B., & Javadpour, S. (2015, November 13). Experimental Study of Mechanical Properties of Additively Manufactured ABS Plastic as a Function of Layer Parameters. *Volume 2A: Advanced Manufacturing*. https://doi.org/10.1115/IMECE2015-52634

Lin, X., Gao, J., Wang, J., Wang, R., Gong, M., Zhang, L., Lu, Y., Wang, D., & Zhang, L. (2021). Desktop printing of 3D thermoplastic polyurethane parts with enhanced mechanical performance using filaments with varying stiffness. *Additive Manufacturing*, *47*. https://doi.org/10.1016/j.addma.2021.102267

Marcel Kuruc, J. H. J. P. J. M. (2024). Research of Layer Thickness and Selected Thermoplastic Materials and their Influence on the Surface Roughness in the Process of Fused Deposition Modeling Technology. *Journal of Electrical Systems*, *20*(4s), 758–765. https://doi.org/10.52783/jes.2099

Martinez, D. W., Espino, M. T., Cascolan, H. M., Crisostomo, J. L., & Dizon, J. R. C. (2022). A Comprehensive Review on the Application of 3D Printing in the Aerospace Industry. *Key Engineering Materials*, *913*, 27–34. https://doi.org/10.4028/p-94a9zb

Minetola, P., Calignano, F., & Galati, M. (2020). Comparing geometric tolerance capabilities of additive manufacturing systems for polymers. *Additive Manufacturing*, *32*. https://doi.org/10.1016/j.addma.2020.101103

Moreno-Núñez, B. A., Abarca-Vidal, C. G., Treviño-Quintanilla, C. D., Sánchez-Santana, U., Cuan-Urquizo, E., & Uribe-Lam, E. (2023). Experimental Analysis of Fiber Reinforcement Rings' Effect on Tensile and Flexural Properties of Onyx™–Kevlar® Composites Manufactured by Continuous Fiber Reinforcement. *Polymers*, *15*(5). https://doi.org/10.3390/polym15051252

Mushtaq, R. T., Iqbal, A., Wang, Y., Cheok, Q., & Abbas, S. (2022). Parametric Effects of Fused Filament Fabrication Approach on Surface Roughness of Acrylonitrile Butadiene Styrene and Nylon-6 Polymer. *Materials*, *15*(15). https://doi.org/10.3390/ma15155206

Nahar, C., & Gurrala, P. K. (2022). Transient thermal finite-element analysis of fused filament fabrication process. *Rapid Prototyping Journal*, *28*(6), 1097–1110. https://doi.org/10.1108/RPJ-05-2021-0104

Nomani, J., Wilson, D., Paulino, M., & Mohammed, M. I. (2020). Effect of layer thickness and cross-section geometry on the tensile and compression properties of 3D printed ABS. *Materials Today Communications*, *22*, 100626. https://doi.org/10.1016/j.mtcomm.2019.100626

O'Connor, H. J., & Dowling, D. P. (2019). Low-pressure additive manufacturing of continuous fiber-reinforced polymer composites. *Polymer Composites*, *40*(11), 4329–4339. https://doi.org/10.1002/pc.25294

Oh, K. C., Yun, B. S., & Kim, J. H. (2022). Accuracy of metal 3D printed frameworks for removable partial dentures evaluated by digital superimposition. *Dental Materials*, *38*(2), 309–317. https://doi.org/10.1016/j.dental.2021.12.012

Oskolkov, A. A., Trushnikov, D. N., & Bezukladnikov, I. I. (2021). Application of induction heating in the FDM/FFF 3D manufacturing. *Journal of Physics: Conference Series*, *1730*(1). https://doi.org/10.1088/1742-6596/1730/1/012005

Qin, Q., Huang, J., & Yao, J. (2019). A real-time adaptive look-ahead speed control algorithm for FDM-based additive manufacturing technology with Hbot kinematic system. *Rapid Prototyping Journal*, *25*(6), 1095–1107. https://doi.org/10.1108/RPJ-11-2018-0291

Quelho de Macedo, R., Ferreira, R. T. L., & Jayachandran, K. (2019). Determination of mechanical properties of FFF 3D printed material by assessing void volume fraction, cooling rate and residual thermal stresses. *Rapid Prototyping Journal*, *25*(10), 1661–1683. https://doi.org/10.1108/RPJ-08-2018-0192

R, R. M., R, V., & S, R. (2021). Experimental analysis on density, micro-hardness, surface roughness and processing time of Acrylonitrile Butadiene Styrene (ABS) through Fused Deposition Modeling (FDM) using Box Behnken Design (BBD). *Materials Today Communications*, *27*. https://doi.org/10.1016/j.mtcomm.2021.102353

Rajpurohit, S. R., & Dave, H. K. (2019). Analysis of tensile strength of a fused filament fabricated PLA part using an open-source 3D printer. *International Journal of Advanced Manufacturing Technology*, *101*(5–8), 1525–1536. https://doi.org/10.1007/s00170-018-3047-x

Ralchev, M., Mateev, V., & Marinova, I. (2021, July 1). Magnetic properties of FFF/FDM 3D printed magnetic material. *2021 17th Conference on Electrical Machines, Drives and Power Systems, ELMA 2021 - Proceedings*. https://doi.org/10.1109/ELMA52514.2021.9503037

Rashed, K., Kafi, A., Simons, R., & Bateman, S. (2022). Fused filament fabrication of nylon 6/66 copolymer: parametric study comparing full factorial and Taguchi design of experiments. *Rapid Prototyping Journal*, *28*(6), 1111–1128. https://doi.org/10.1108/RPJ-06-2021-0139

Rupal, B. S., Anwer, N., Secanell, M., & Qureshi, A. J. (2020). Geometric tolerance and manufacturing assemblability estimation of metal additive manufacturing (AM) processes. *Materials and Design*, *194*. https://doi.org/10.1016/j.matdes.2020.108842

Shakeri, Z., Benfriha, K., Shirinbayan, M., Ahmadifar, M., & Tcharkhtchi, A. (2021a). Mathematical modeling and optimization of fused filament fabrication (Fff) process parameters for shape deviation control of polyamide 6 using taguchi method. *Polymers*, *13*(21). https://doi.org/10.3390/polym13213697

Shakeri, Z., Benfriha, K., Shirinbayan, M., Ahmadifar, M., & Tcharkhtchi, A. (2021b). Mathematical Modeling and Optimization of Fused Filament Fabrication (FFF) Process Parameters for Shape Deviation Control of Polyamide 6 Using Taguchi Method. *Polymers*, *13*(21), 3697. https://doi.org/10.3390/polym13213697

Shakeri, Z., Benfriha, K., Zirak, N., & Shirinbayan, M. (2022). Mechanical strength and shape accuracy optimization of polyamide FFF parts using grey relational analysis. *Scientific Reports*, *12*(1), 13142. https://doi.org/10.1038/s41598-022-17302-z

Sharma, S., Datta, S., Roy, T., & Mahapatra, S. S. (2023). Study of parametric interaction during fused filament fabrication (FFF) using interpretive structural modelling (ISM) followed by experimental analysis. *Rapid Prototyping Journal*, *29*(10), 2232–2256. https://doi.org/10.1108/RPJ-03-2023-0092

Singh, J., Singh, R., & Singh, H. (2016). Repeatability of linear and radial dimension of ABS replicas fabricated by fused deposition modelling and chemical vapor smoothing process: A case study. *Measurement: Journal of the International Measurement Confederation*, *94*, 5–11. https://doi.org/10.1016/j.measurement.2016.07.064

Singh, M., & Bharti, P. S. (2022). Grey relational analysis based optimization of process parameters for efficient performance of fused deposition modelling based 3D printer. *Journal of Engineering Research*. https://doi.org/10.36909/jer.ICMET.17159

Song, P. S., Hwang, S., & Sheu, B. C. (2005). Strength properties of nylon- and polypropylene-fiber-reinforced concretes. *Cement and Concrete Research*, *35*(8), 1546–1550. https://doi.org/10.1016/j.cemconres.2004.06.033

Temiz, A. (2024). A response surface methodology investigation into the optimization of manufacturing time and quality for FFF 3D printed PLA parts. *Rapid Prototyping Journal*, *30*(10), 2007–2020. https://doi.org/10.1108/RPJ-01-2024-0004

Terekhina, S., Skornyakov, I., Tarasova, T., & Egorov, S. (2019). Effects of the Infill Density on the Mechanical Properties of Nylon Specimens Made by Filament Fused Fabrication. *Technologies*, *7*(3). https://doi.org/10.3390/technologies7030057

Valerga Puerta, A. P., Fernandez-Vidal, S. R., Batista, M., & Girot, F. (2020). Fused deposition modelling interfacial and interlayer bonding in PLA post-processed parts. *Rapid Prototyping Journal*, *26*(3), 585–592. https://doi.org/10.1108/RPJ-06-2019-0176

Vanaei, H. R., Khelladi, S., & Tcharkhtchi, A. (2022). Roadmap: Numerical-Experimental Investigation and Optimization of 3D-Printed Parts Using Response Surface Methodology. *Materials*, *15*(20), 7193. https://doi.org/10.3390/ma15207193

Vazquez-Martinez, J. M., Piñero, D., Salguero, J., & Batista, M. (2020). Evaluation of the joining response of biodegradable polylactic acid (PLA) from fused deposition modeling by infrared laser irradiation. *Polymers*, *12*(11), 1–11. https://doi.org/10.3390/polym12112479

Vyavahare, S., Kumar, S., & Panghal, D. (2020). Experimental study of surface roughness, dimensional accuracy and time of fabrication of parts produced by fused deposition modelling. *Rapid Prototyping Journal*, *26*(9), 1535–1554. https://doi.org/10.1108/RPJ-12-2019-0315

Yang, T. C., & Yeh, C. H. (2021). Characteristics of Unidirectional Green Wood Fiber/Polylactic Acid Composite Parts Printed with Various Layer Thicknesses by Fused Filament Fabrication. *3D Printing and Additive Manufacturing*, *8*(5), 322–330. https://doi.org/10.1089/3dp.2020.0210

Yunus, N., Rashid, A. A., Azmi, L. L., & Abu-Hassan, M. I. (2005). Some flexural properties of a nylon denture base polymer. *Journal of Oral Rehabilitation*, *32*(1), 65–71. https://doi.org/10.1111/j.1365-2842.2004.01370.x